

High Fracture Toughness Acrylic-Polyurethane Based Graft-Interpenetrating Polymer Networks for Transparent Applications

Nima Alizadeh^{1,2}, Mehul Barde^{1,2}, Michael Minkler¹, Asha-Dee Celestine³, Vinamra Agrawal³,
Bryan Beckingham¹, Maria L. Auad^{1,2*}

¹Department of Chemical Engineering, Auburn University, US

²Center for Polymers and Advanced Composites, Auburn University, US

³Department of Aerospace Engineering, Auburn University, US

Abstract:

Transparent materials with robust mechanical properties are essential for numerous applications and require careful manipulation of polymer chemistry. Here, polyurethane (PU) and acrylic-based copolymers out of styrene are utilized to synthesize transparent polyurethane-acrylic graft-interpenetrating polymer networks (graft-IPNs) for the first time. In these materials, PU imparts greater flexibility, while the acrylic copolymer increases rigidity and glass transition temperature of the graft-IPN. Kinetics of the graft-IPN synthesis is monitored using Fourier transform infrared spectroscopy (FT-IR), and ¹H nuclear magnetic resonance spectroscopy (¹H-NMR) through the conversion of the isocyanate group. System compatibility, degree of phase separation, and material transparency were evaluated using a transmission electron microscope (TEM) and UV-visible spectroscopy. Overall, higher compatibility is observed at a higher percentage of styrene in the

This article has been accepted for publication and undergone full peer review but has not been through the copyediting, typesetting, pagination and proofreading process which may lead to differences between this version and the Version of Record. Please cite this article as doi: 10.1002/pi.6149

acrylate copolymer. The thermomechanical properties of the IPN networks were quantified by dynamic mechanical analysis (DMA) to assess the effect of the acrylic copolymer content on fracture toughness of the resulting graft-IPN. The high fracture toughness of the graft-IPN, coupled with excellent transparency, demonstrates the potential of this system for high-performance applications.

*To whom the correspondence should be addressed

Keywords: Interpenetrating polymer networks (IPN), polyurethane, acrylic-based copolymers, NMR polymerization, thermomechanical, fracture toughness, viscoelastic properties

Introduction

Transparent polymeric materials with high impact resistance demonstrate good potential for a wide range of applications such as safety enclosures, aerospace applications, windshields, safety goggles, and many more.^{1,2} Traditionally, glass has been used as the staple transparent material in general consumer and engineering applications.^{3,4} However, glass has high density and low impact resistance restricting its use in high-performance applications.⁵ Recently, the development of transparent and high impact resistance polymeric materials for engineering applications has attracted widespread attention.⁶ Ease of processing, low density, tunable mechanical properties, excellent impact resistance, and fracture toughness of these new polymeric materials are some of the significant reasons which make them suitable candidates for advanced applications.^{6,7}

While the direct blending of polymers is one method for formulating polymers with enhanced properties,⁸ the final mixing process presents challenges due to the tendency for phase separation to occur.^{9,10} To overcome phase separation between dissimilar polymers while also improving the compatibility of the solid-state material, different polymerization processes have been developed including graft and block copolymers and interpenetrating polymer networks (IPNs).¹¹

Interpenetrating polymer networks are classified as a multi-component system where one polymer is synthesized in the presence of another.¹² Most multi-component polymeric materials form immiscible phases due to low entropy of mixing.¹² IPNs attract much attention in multi-component materials due to their physical entanglement, which brings about forced compatibility into the system, therefore increasing miscibility between the two phases.¹² Synthetic method, degree of

Accepted Article

polymerization, and degree of crosslinking are factors influencing the final morphology of IPNs.¹³ There are many different ways to classify interpenetrating polymer networks based on their physical and chemical properties. A full-IPN is one kind of interpenetrating polymer network where both polymers are crosslinked, in semi-IPN's only one of the polymer is crosslinked, while the other polymer is linear,¹⁴ and in graft-IPN both polymers are crosslinked, and a controlled amount of bonding is allowed between the two polymers.^{11, 15} Latex IPN is another kind of IPN where the IPN is in the form of latex; therefore it is a so-called interpenetrating elastomeric network (IEN).^{12, 16} IPNs can also be classified as simultaneous or sequential based on the synthetic method applied. In sequential IPNs, the first polymer network is formed, swollen in the monomers of the second polymer, which is then polymerized, forming the second polymer network. In simultaneous polymerization, polymerization of the two polymer networks occurs at the same time, and no interfering reactions occur.^{10, 17, 18}

In the literature, numerous groups have studied IPN systems, such as Millar et al.¹⁹, and Aylsworth and Edison^{10, 12, 20-22}, who have utilized different monomers to investigate various aspects of IPNs. Extensive research on this topic has also been performed by the authors^{23, 24}. In previous studies, the effect of different parameters such as curing profile, the composition of two polymer systems^{5, 7, 25-27}, the substitution of aliphatic and aromatic isocyanate²⁵, the impact of the molecular weight of diol⁷, simultaneous and sequential polymerization method²⁵, and using chemical bonds to synthesize graft-IPNs²⁸, have been studied. Overall, these studies suggested IPNs containing aliphatic isocyanate with 1400 g/mol diol and following a sequential synthetic method, and

Accepted Article

chemical bonds between the two phases presented better transparency and thermomechanical properties due to reduced phase separation from improved compatibility provided between the two phases. It was also observed that utilizing PU with an acrylic copolymer, such as PMMA based copolymers, led to an improvement of $\approx 150\%$ in fracture toughness of the acrylic copolymer. The enhancement in phase compatibility of the IPNs was also addressed.^{6, 25, 28-33}

In this work, the impact of varying the acrylic copolymer precursors and the chemical bonding between the two polymer networks is investigated towards the overall goal of synthesizing novel graft-IPNs with excellent compatibility, transparency, and superior fracture toughness. For the first time, styrene, as one of the acrylic copolymer monomers, was utilized in the graft-IPN system. Two methods were utilized to monitor the polymerization of the two phases in the IPN systems. The compatibility of the two phases was evaluated using a transmission electron microscope (TEM), dynamic mechanical analyzer (DMA), and UV-Vis spectroscopy, while SEM and quasi-static fracture tests were used to investigate the mechanism of the fracture toughness.

Experimental section

Materials

In this work, the polyurethane (PU) phase was synthesized from the following compounds: 2-ethyl-2-(hydroxymethyl)-1,3-propanediol (TRIOI, MW=134.18 g/mol, crosslinker) purchased from Acros Organics, poly(tetramethylene ether) glycol (PTMG, MW=approximately 1400 g/mol) purchased from Aldrich, hexamethylene diisocyanate (DCH) purchased from TCI, and dibutyltin dilaurate (DBTDL) and triphenylbismuth (TPB) as catalysts purchased from Pfaltz & Bauer and

Alfa Aesar, respectively. Ethyl acetate, purchased from Alfa Aesar, was the solvent used for the catalyst mixture. To synthesize the acrylic copolymer, styrene was purchased from Alfa Aesar, bisphenol A bis(2-hydroxy-3-methacryloxypropyl) ether (BisGMA) was purchased from Esstech, and 2,2'-azobis(2-methyl-propionitrile) (AIBN, thermal initiator) was purchased from Matrix Scientific. 4Å molecular sieves, purchased from Alfa Aesar, were used to remove the moisture from DCH, styrene, TRIOL, and PTMG.

Methods

Synthesis of graft-IPNs

TRIOL (0.19 eq) and PTMG (0.12 eq) were heated to 60°C, and the molten TRIOL and PTMG were mixed with a stirrer. Next, DCH (0.31 eq + calculated amount of DCH to react with BisGMA), was added to the mixture, and the mixture was stirred. The PU phase accounted for 25 wt% of the final composition for all specimens.

For the second phase, different percentages of BisGMA were dissolved into styrene, and then AIBN (1 wt% of total co-monomer mass) was dissolved into the mixture. Then PU monomers and acrylic phase monomers were mixed. 600 µL DBTDL per 50 grams of PU (0.02 M Ethyl acetate solution) and 600 µL TPB (0.001 M Ethyl acetate solution) were added to the monomer mixture at the end of this stage for the poly-addition polymerization of the PU phase. Finally, the mixture

was cured in closed aluminum molds for 24 hours at 40°C, followed by 24 hours at 60°C and finally 24 hours at 80°C.

Figure 1 shows the polyaddition polymerization chemistry of the polyurethane network. The simple schematic of the reaction occurring for acrylic copolymer synthesis and IPN network structure is shown in Figure 2 and Figure 3, respectively.

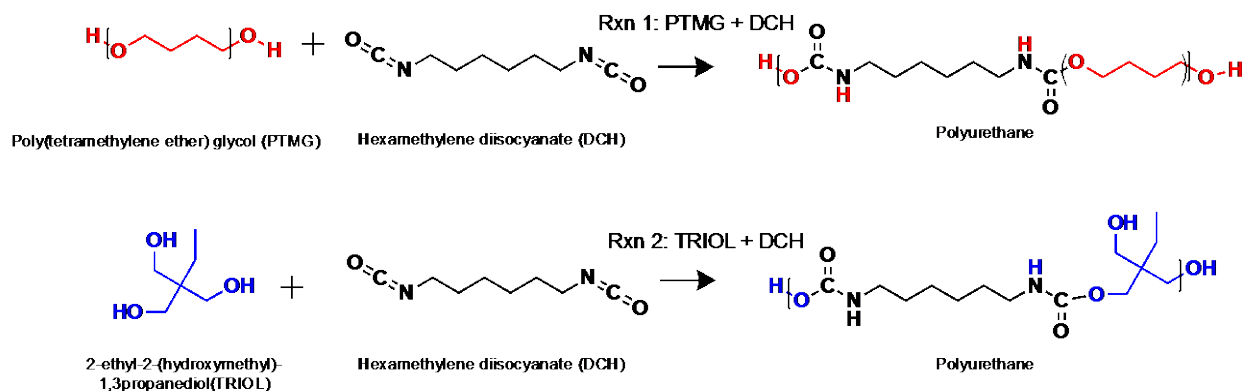


Figure 1. Two polyaddition polymerization reactions that form the polyurethane phase. (Top) reaction between PTMG and DCH and (Bottom) reaction between TRIOL and DCH

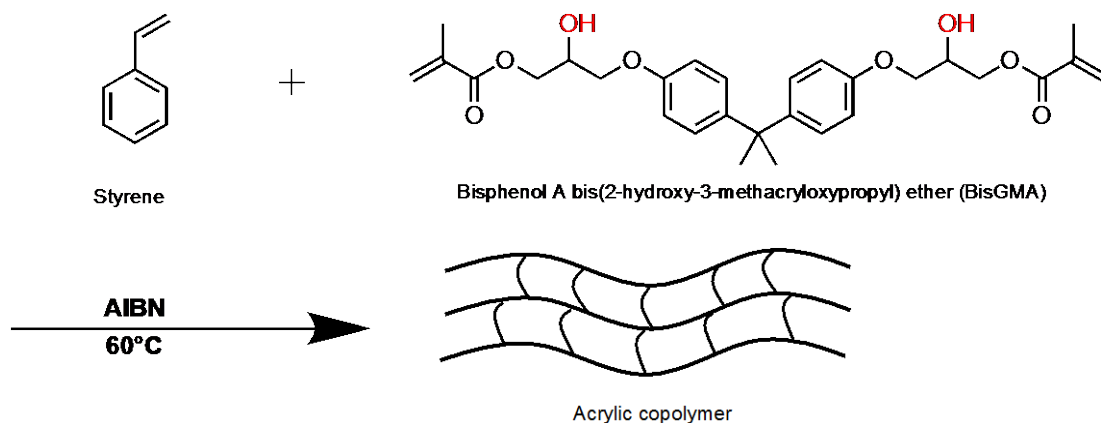


Figure 2. Free radical polymerization of the acrylic copolymer from styrene and BisGMA.

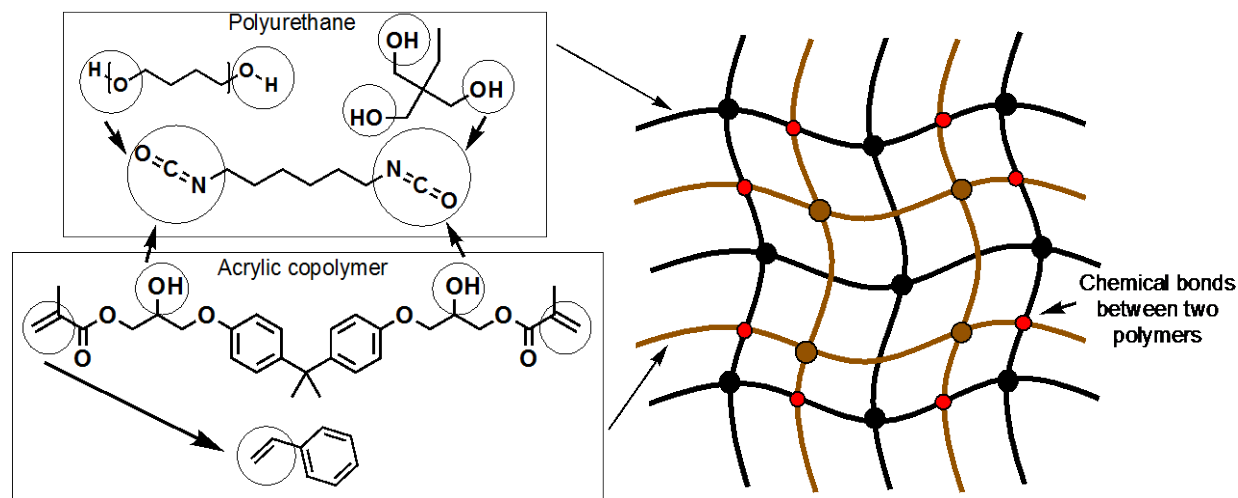


Figure 3. Simple schematic of IPN network structure

Characterization

Fourier transform infrared spectroscopy (FT-IR) was performed with a Nicolet 6700 FT-IR spectrometer from Thermo Scientific (USA) in attenuated total reflection (ATR) infrared mode. FTIR experiments were performed from 400-4000 cm^{-1} wavenumber with 64 scans and using a 4 cm^{-1} resolution.

Low-field ^1H nuclear magnetic resonance spectroscopy (LFNMR) was performed on an Oxford Pulsar 60 MHz (1.4 Tesla) NMR spectrometer using Wilmad class B eight-inch high-throughput tubes (5 mm outer diameter, 4 mm internal diameter). The ^1H NMR experiment was conducted as an arrayed experiment in the Oxford Spin flow Software with 64 scans/run, a recycle delay of 2 seconds and a spectral width of 50,000 Hz. This combination of the parameters yields an

approximate sampling time of 5 minutes and 48 seconds per spectrum. The spectra were analyzed using Mnova software.

A Zeiss EVO 50 variable pressure scanning electron microscope (SEM) with digital imaging and EDS (with the IPNs sputter-coated with an EMS 550X auto sputter coating device with carbon coating attachment) was used to study the surface morphology of the specimens. The specimens were immersed in the liquid nitrogen, broken, and the fracture events visualized using SEM. A Zeiss EM 10C 10CR transmission electron microscope (TEM) was used to examine the interior morphology of the samples. Samples were stained using a 2.5% aqueous solution of osmium tetroxide (OsO_4) for one week, as reported by Kato prior to microtoming.³⁴ A Cary 60 UV/Vis spectrometer from Agilent (USA) was used to verify the transparency of the samples (250-800 nm wavelength).

TA Instruments RSA 3 dynamic mechanical analyzer (DMA) was used for studying the thermomechanical properties of the IPNs. Flexural tests were performed on the samples from 25-200°C with a sinusoidal strain amplitude of 0.1% and 0.1 Hz frequency, and a 5°C/min heating rate.

The fracture toughness properties of specimens were characterized using quasi-static fracture tests performed in a 3-point bending condition following ASTM D5045.³⁵ Equations 1, 2, and 3 were used to calculate the plane-strain fracture toughness K_{Ic} , where a is crack length, W is specimen width, B is specimen thickness, and $0 < x < 1$.

$$K_{Ic} = \left(\frac{P_Q}{BW^{3/2}} \right) f(x) \quad [1]$$

$$f(x) = 6x^{1/2} \frac{[1.99-x(1-x)(2.15-3.93x+2.7x^2)]}{(1+2x)(1-x)^{3/2}} \quad [2]$$

$$x = \frac{a}{w} \quad [3]$$

Cured specimens were cut to bars of dimensions 55 mm x 12 mm x 3 mm using Boss Laser LS 3655. An edge notch 4 mm in length was cut into the samples with a saw, and the edge tip subsequently sharpened with a razor blade. The single edge notched bend (SENB) test was performed on the specimens using an Instron 5565 with 1 kN static load cell. The load and displacement data were recorded up to crack initiation and during stable crack growth. The load at crack initiation (P) was used to calculate K_{Ic} . MATLAB was utilized to calculate K_{Ic} with Equations 1, 2, and 3, and at least five specimens were tested for each composition.³¹

Results and discussion

Analysis of isocyanate conversion by FTIR measurements

The compositions (using a 10 g sample basis) of synthesized materials investigated with FTIR and NMR spectroscopy and their corresponding nomenclature are shown in Table 1. The isocyanate conversion (NCO) was studied using FTIR spectroscopy. The measurement is based on the decay in intensity of the peak assigned to isocyanate absorption during polymerization. The absorption peak of the isocyanate group is assigned to approximately 2270 cm^{-1} . C-H stretch absorption happening within 2850-3000 cm^{-1} was used as an internal standard due to the constant concentration of this band during the reaction.³⁶ The isocyanate conversion was calculated with the help of equation 4³⁷ shown below:

$$p = 1 - \frac{\frac{A_{NCO}}{A_{CH_2}}}{\left(\frac{A_{NCO}}{A_{CH_2}}\right)_0} \quad [4]$$

where p is the isocyanate conversion, A_{NCO} is the integrated absorbance for the isocyanate group. A_{CH_2} is the integrated absorbance for the C-H stretch absorption and $\left(\frac{A_{NCO}}{A_{CH_2}}\right)_0$ is the relative absorbance extrapolated to time zero.

Table1. Prepared sample compositions used for FTIR and NMR spectroscopy

Sample	Polyurethane			Acrylic copolymer	
	25 wt%			75 wt%	
	PTMG wt%	TRIOL wt%	DCH wt%	Styrene wt%	BisGMA wt%
PU-PT	70.8	7.2	22	--	--
PU-P	89	--	11	--	--
PU-B	--	--	24.7	--	75.3
PU-PTB	14.2	1.4	24.2	--	60.2
IPN80/20	16.9	1.7	9.9	57.2	14.3
COP80/20	--	--	--	80	20

FTIR spectra for PU-PT at 0, 18, 36, 64 min, and three days are shown in Figure 4, where the isocyanate absorption peak (2270 cm^{-1}) decreases during polymerization while the C-H stretch absorption peak ($2800\text{-}3000\text{ cm}^{-1}$) remains constant. This indicates the isocyanate groups react with the hydroxyl group of the TRIOL and PTMG to form the PU network as expected.

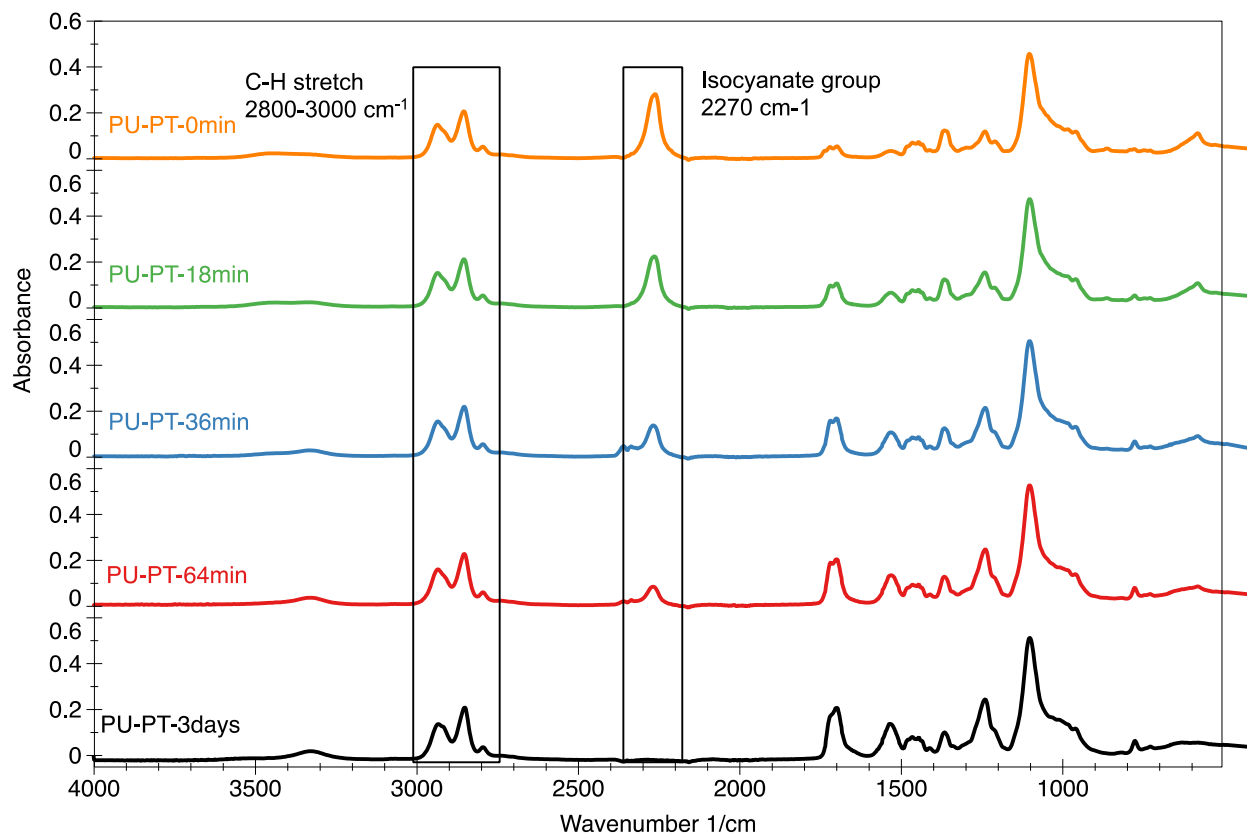


Figure 4. FTIR spectra of the PU-PT sample at five different times

The isocyanate conversion versus time data extracted from the FTIR spectra is shown in Figure 5. While initial polymerization rates across the series are similar (except for PU-B), PU-P is the first to reach near completion. PU-B clearly shows the slowest polymerization rate, likely due to the secondary hydroxyl groups in the BisGMA and the corresponding steric hindrance compared to the PTMG primary hydroxyl group.³⁸ PU-PTB shows a higher polymerization rate in comparison to PU-PT due to the presence of BisGMA which provides more hydroxyl groups into the system.

PU-PT and IPN80/20 follow the same trend due to the dominant behavior of PU in isocyanate conversion and steric effect of acrylic copolymer into the IPN system.

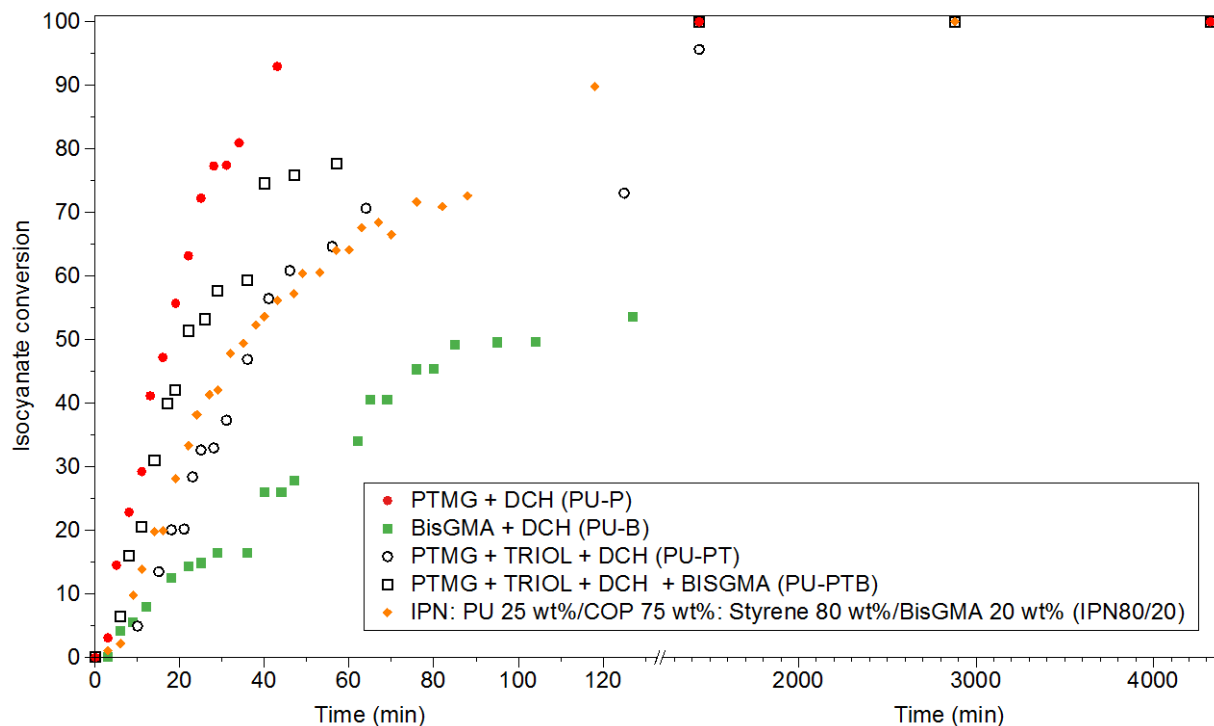


Figure 5. Isocyanate conversion of PTMG + TRIOL + DCH (PU-PT) , IPN80/20 and its constituents.

FTIR spectroscopy was also utilized for pure acrylic copolymer with 20 wt% BisGMA and 80 wt% styrene (COP80/20) to characterize their free radical polymerization at 60°C, which forms the second polymer network in IPN80/20. Samples were cured for 24 hours at 60°C and then cured for 24 hours at 80°C and their FTIR spectra obtained at the beginning of the synthesis and after two days of curing (Figure 6). Peaks at 774 and 908 cm^{-1} corresponding to the out-of-plane (oop)

bending of =C-H and at 1600-1660 cm^{-1} corresponding to C=C can be used to track polymerization. Both of these peaks decrease during free radical polymerization due to the consumption of double bonds. Moreover, a peak corresponding to sp^3 C-H stretching appears after two days of curing in range of 2850-3000 cm^{-1} as additional confirmation of consumption of C=C-H to form sp^3 C-H.

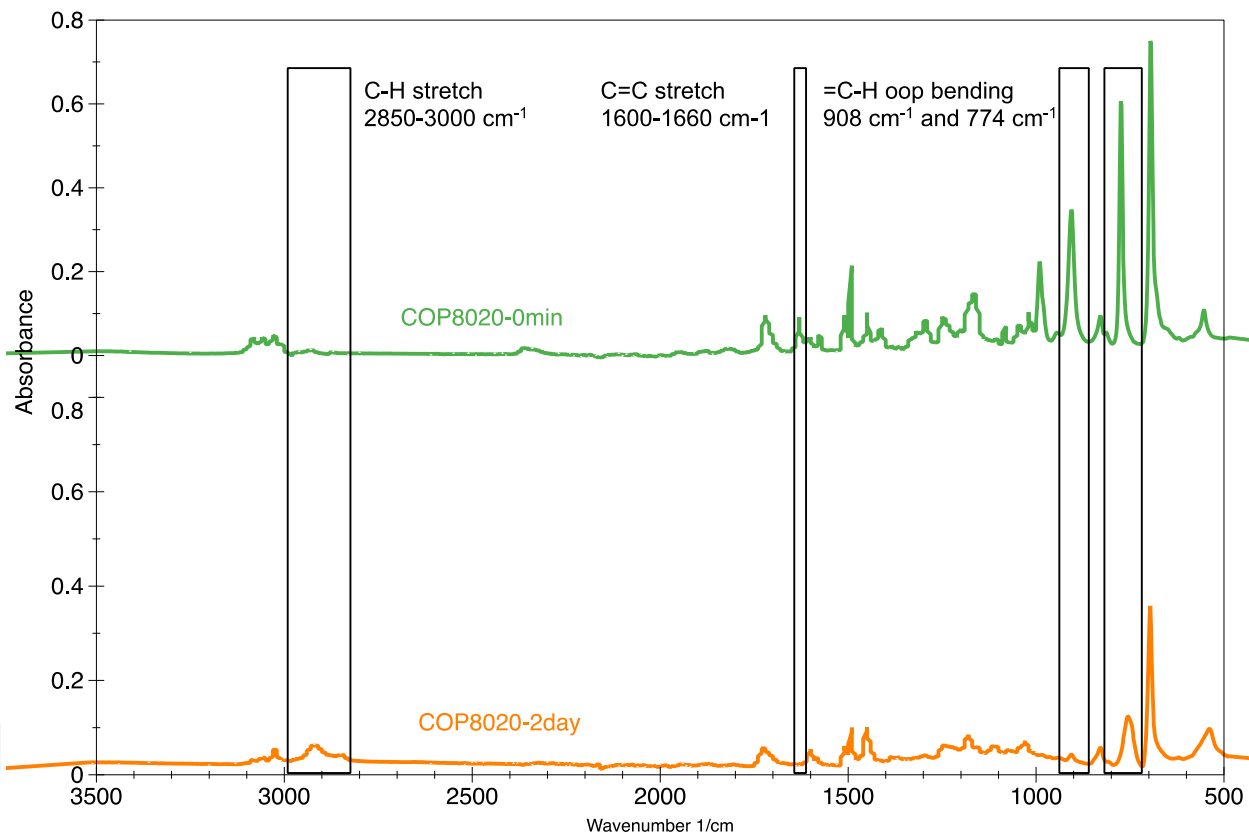


Figure 6. FTIR spectra of the acrylic copolymer at 0 min (top) and after two days of curing (bottom).

Analysis of isocyanate conversion via Low-field NMR Spectroscopy

Reaction progress for PU-P and PU-PT were also tracked using an Oxford Instruments Pulsar 60 MHz NMR spectrometer. Briefly, an initial spectrum of PTMG was collected prior to the addition of DCH and two drops of each catalyst, DBTDL and TPB, dissolved in ethyl acetate. The reaction mixture was agitated via stirring with copper wire and manual shaking of the tube before being placed into the probe bore. The spectrometer was tuned and matched to the sample, and then an arrayed experiment was commenced. Note that the lag time (time from the addition of the catalyst to start of the NMR spectroscopy tracking experiment) was accounted for in both the reaction progress diagram, Figure 7, and the subsequent data analysis.

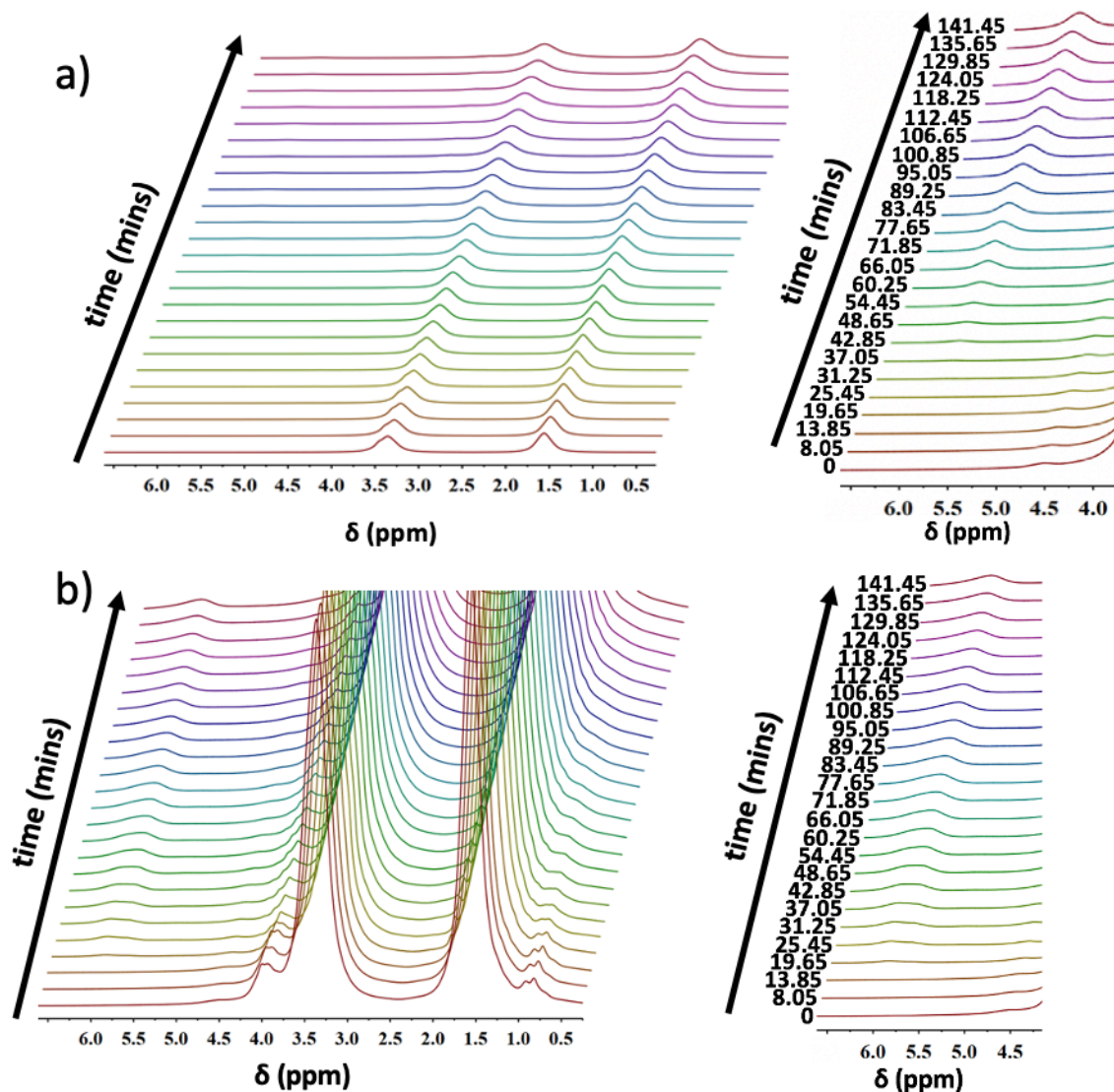


Figure 7. (left) NMR spectra from in-situ reaction monitoring of a) PU-P and b) PU-PT with (right) spectra enlarged to show polyurethane linkage peak.

Tetramethylsilane (a standard additive used to align most 1D ^1H NMR spectra) was not used here to eliminate any possible interactions with the reaction media. Instead, all spectra were shifted based on the far right peak attributed to the PTMG backbone of the PU-P (1.56 ppm).³⁶ This peak

also served as an internal calibration standard as the underlying protons associated with this peak (for both systems) are conserved; for the PU-PT system, the TRIOL aliphatic arm also contributes to this peak, so five additional protons are accounted for as shown in Figure 8.

Unfortunately, due to the spectral overlap in the aliphatic region of the NMR spectra, Figure 7, the consumption of hydroxyl groups could not be tracked directly. However, in both cases, the formation of urethane linkages can be traced through the formation of N-H protons. By utilizing this method, we combine the advantages of more traditional differential scanning calorimetry reaction tracking through heat evolution and that of the FTIR spectroscopy through bond identity, as discussed in this paper. Furthermore, as has been discussed elsewhere, an additional advantage of the low-field NMR spectrometer used here is the soft-lock algorithm, which eliminates the need for deuterated solvents and allows for examination of protons without any adulteration of the reaction media.³⁹

As shown in Figure 7, the peak at 5.94 ppm grows in intensity over time due to the continuous formation of secondary amine peaks as urethane linkages are formed. In the case of PU-P, each urethane linkage is strictly from the consumption of -OH groups on the PTMG chain ends. However, for PU-PT this metric of conversion is complicated by the presence of additional hydroxyl groups on the arms of the TRIOL. Nonetheless, the overall conversion to isocyanate linkages was tracked as a function of peak area and number of protons via Equation 5,

$$\text{Conversion} = 100 \times \frac{A_{5.94}N_{1.56}}{A_{1.56}N_{5.94}} \quad [5]$$

Where A_i is the peak areas at i ppm, and N_j is the number of protons associated with the peak at j ppm. Peak areas (A_i) were extracted from Gaussian fits to the peaks after spectral shifting, automatic phasing, and automatic baselining in the Mnova software. For PU-P $N_{1.56}=76.665$ and $N_{5.94}=2.0157$, while for PU-PT $N_{1.56}=81.70375$ and $N_{5.94}=6.04704$. These values are calculated for each chemistry from the reaction stoichiometry and chemical structures shown in Figure 8.

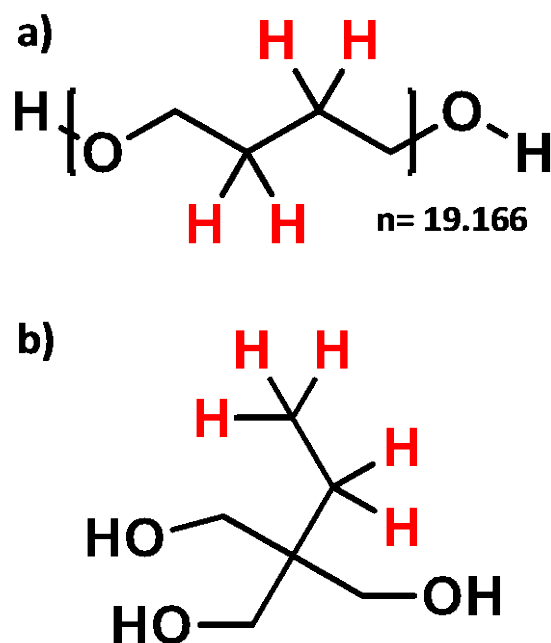


Figure 8. Protons used in the calculation of $N_{1.56}$ are highlighted in red for a) PTMG and b) TRIOL.

In the case of PU-P, this analysis assumes only one DCH molecule is present in the “repeat unit” of the network, while PU-PT has the potential for up to three DCH molecules; two amine protons

and six amine protons respectively. This is important as the network is complicated by the availability of hydroxyl groups from these two different mer units. Extracted conversion versus time data and their comparison by FTIR data are shown in Figure 9.

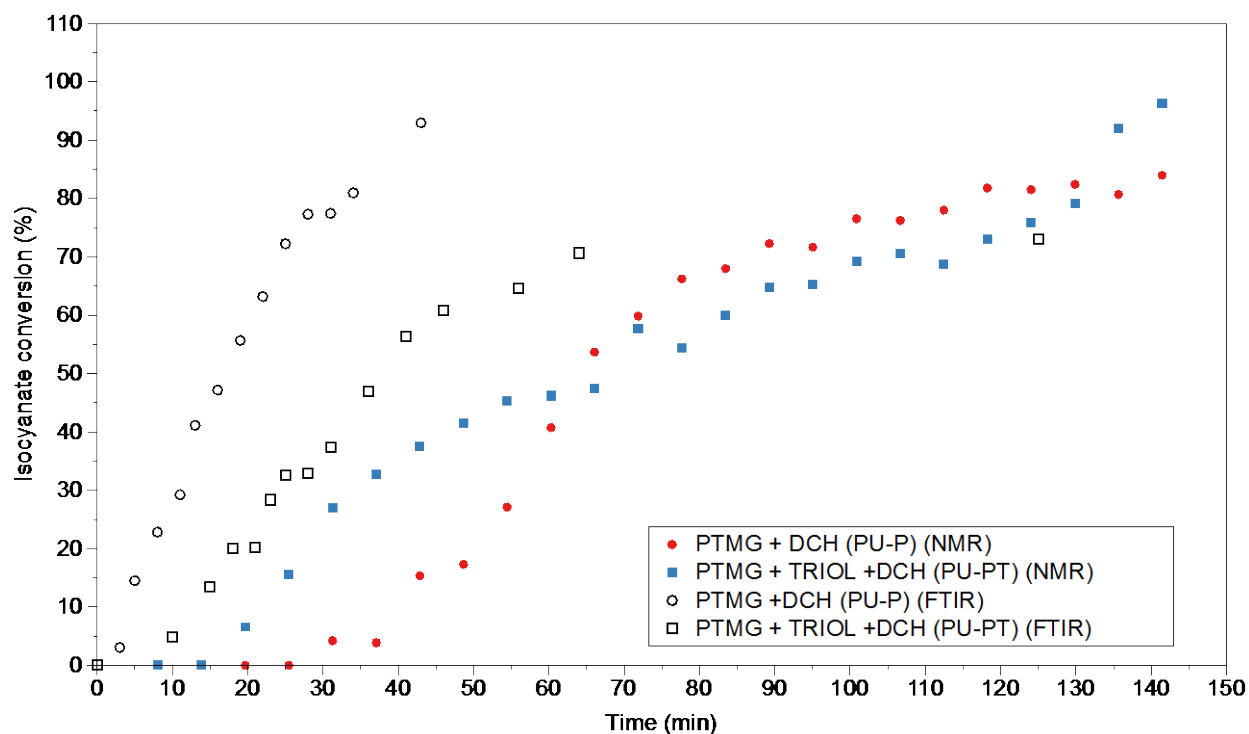


Figure 9. Reaction progress for both systems as a function of isocyanate conversion.

As shown in Figure 9, both systems exhibit a lag time at the beginning of the reaction in the NMR instrument, which we attribute to the low reaction rate at room temperature as the reaction media approaches the spectrometer operating temperature of 37 °C. However, the reaction can be effectively tracked over time as the DCH is incorporated within the polymeric structure, and

isocyanate groups are converted into secondary amines within the urethane linkages. While the data points appear to be non-continuous, it is essential to note that the spectrometer is averaging the signal over 64 scans that are acquired over a cycle time of approximately 5 minutes and 48 seconds; i.e., the resulting isocyanate conversion is time-averaged. Additionally, the conversion in each case reaches a maximum at approximately the same time as extracted from FTIR spectroscopy after accounting for the thermal lag time. Overall, we find this method to provide adequate and facile means to track both reaction progress and bond-specific formation.

Network morphology

A series of IPNs with different styrene to BisGMA content in the acrylic network were synthesized, and their morphology examined with TEM (Figure 10). The lines observed in Figure 10. a, b , and c are tool marks produced during the microtoming procedure. The pure acrylic copolymer (Figure 10a) shows a homogeneous dispersion of the polymeric component throughout the copolymer sample and is utilized as the control experiment for comparisons. No clear OsO₄ stained domains are observed in this sample. In the IPN samples, the polyurethane regions become black after sample staining, while the acrylic phase does not interact with OsO₄ and remains clear. Figures 10b, 10c, and 10d display TEM images of IPN with 70, 80, and 90 wt% of styrene, respectively. In Figure 10b, a distinct black domain is observed in the sample due to the incompatibility of the two polymers containing 70 wt% styrene. However, the IPN composed of 80 wt% styrene shows a fine dispersion of the two polymers with no well-defined domains in the image. As described by

Bird et al., the absence of defined domain shapes indicates a good interpenetration of two phases.²⁵

The finest phase domains of the samples, as observed by TEM, typically indicates the highest level of interpenetration between the two polymers.³⁰ Figure 10d corresponds to the IPN system with 90 wt% styrene and demonstrates good interpenetration between two polymers with less phase separation in comparison to sample with 70 wt% of styrene. The smaller size and thereby higher mobility of styrene in comparison to BisGMA within the polyurethane network likely improve swelling of the forming polyurethane network and decreases phase separation.

It was also observed that utilizing a linear isocyanate (such as DCH) has a positive effect on the compatibility of two phases.²⁵ Ballesterio et al. also used TEM to study the impact of post-curing processes on domain size and interpenetration of polyurethane similar with PMMA and observed better dispersion between two polymers after post-curing due to the additional chemical bonds formed between the two polymer networks during this process.²⁸

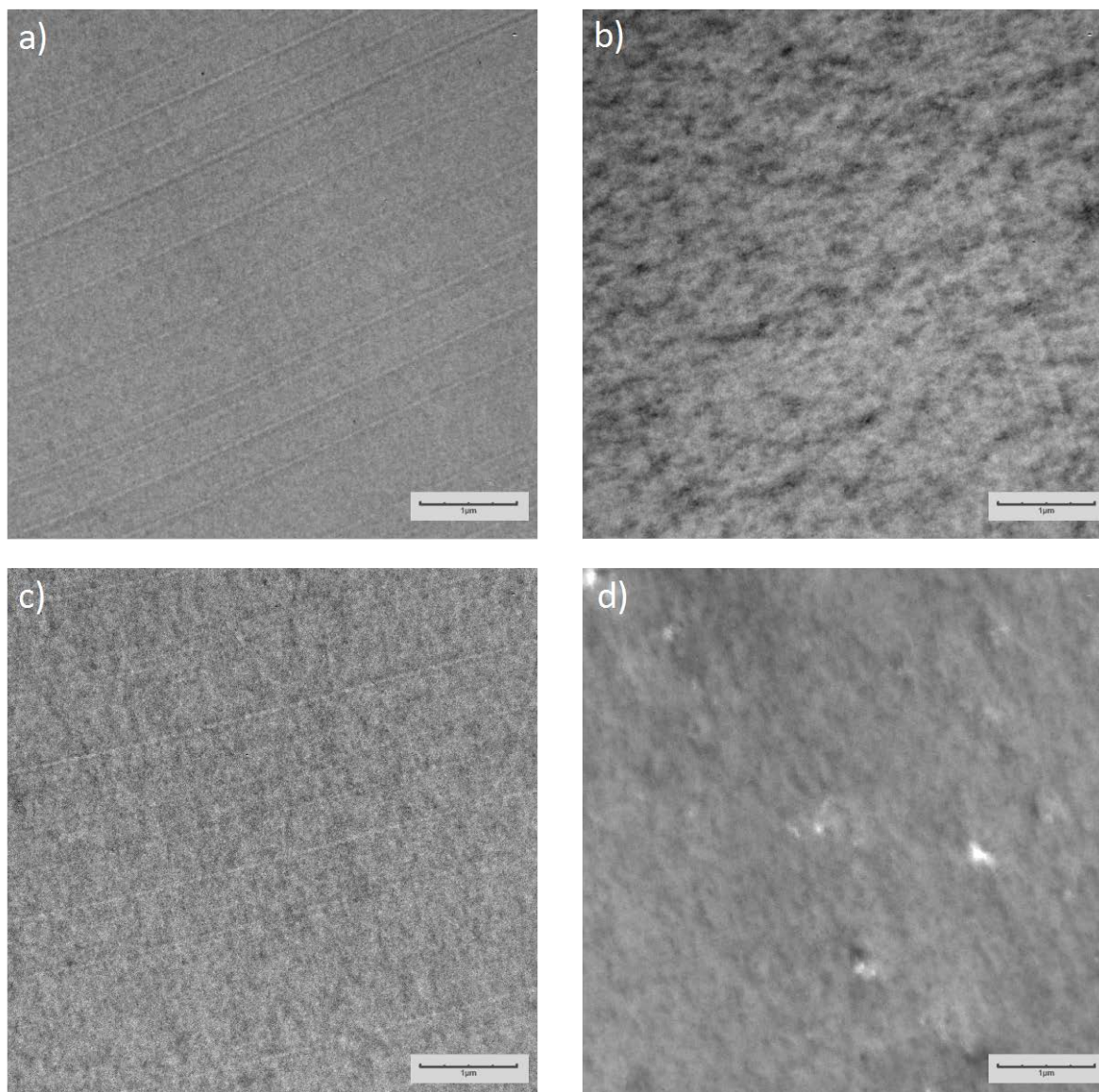


Figure 10. TEM images of IPN with 25 wt% PU and 75 wt% acrylic copolymer with different copolymer composition: a) copolymer: styrene 80 wt%/ BisGMA 20 wt% b) IPN: styrene 70 wt%/ BisGMA 30 wt% c) IPN: styrene 80 wt%/ BisGMA 20 wt% d). IPN: styrene 90 wt%/ BisGMA 10 wt%

Degree of transparency

IPN transparency was investigated using UV-Visible spectrophotometry with the results for the IPNs of varied styrene to BisGMA composition shown in Figure 11. Transparency is a strong function of composition as samples with 50 wt% styrene show almost no transparency while increasing styrene content leads to increasing transparency. For samples IPN: styrene 80 wt%/ BisGMA 20 wt% (Figure 10.c) and IPN: styrene 90 wt%/ BisGMA 10 wt% (Figure 10.d), the domain sizes are below the 380nm on average; for these samples, good transparency was observed. In the case of the IPN: styrene 70 wt%/ BisGMA 30 wt% (Figure 10.b), it shows the domain in the range of the light wavelength, and the transmittance is considerably reduced. Ultimately, samples with 80 and 90 wt% of styrene show transmittance values close to 100 % in the visible light wavelength region, indicating good compatibility between phases.

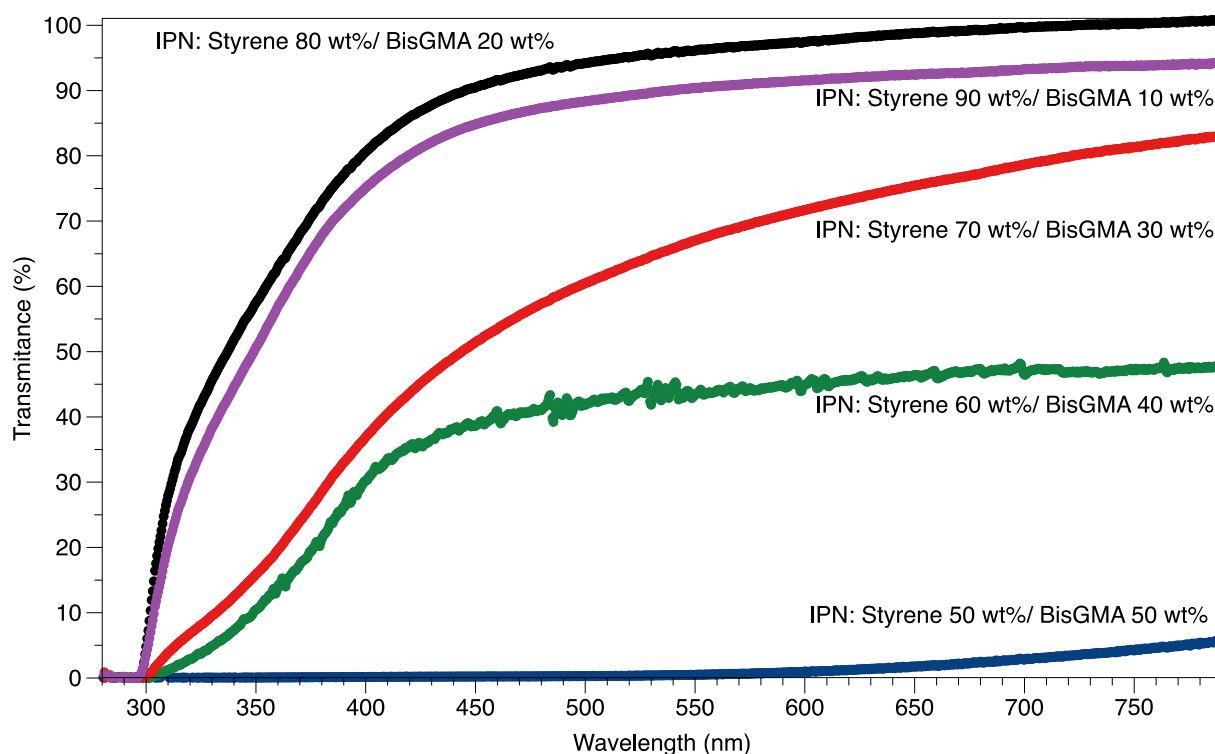


Figure 11. UV-Visible spectra of the IPNs with 25 wt% PU and 75 wt% acrylic copolymer with different copolymer composition

Thermo-mechanical characterization

Thermo-mechanical properties of the synthesized IPNs were evaluated using dynamic mechanical analysis (DMA). Figure 12a shows the storage modulus of the samples vs. temperature; samples with a higher percentage of styrene show higher initial moduli due to better compatibility between the two phases. Figure 12b shows the $\tan \delta$ results of the samples vs. temperature. The 50 wt% styrene IPN shows two peaks in $\tan \delta$, indicating the presence of two glass transition temperatures, and is an indication of phase separation between the polyurethane and acrylic copolymer constituents. The gap between the two peaks decreases with increasing styrene content, due to the higher compatibility between two phases. The 70 wt% styrene IPN (Figure 12b) exhibits a flat peak in $\tan \delta$, due to improving compatibility but the remaining presence of phase separation. The IPN with 80 wt% of the styrene shows only one peak in its $\tan \delta$ demonstrating better compatibility between the two IPN constituents as observed with TEM and UV-vis spectroscopy. The peak becomes sharper for the 90wt% styrene IPN sample, further verifying enhanced phase compatibility. Broader peaks in samples with a lower percentage of styrene suggest that there are several relaxation mechanisms in the systems, which are more heterogeneous at the microscopic scale.^{25, 28, 40}

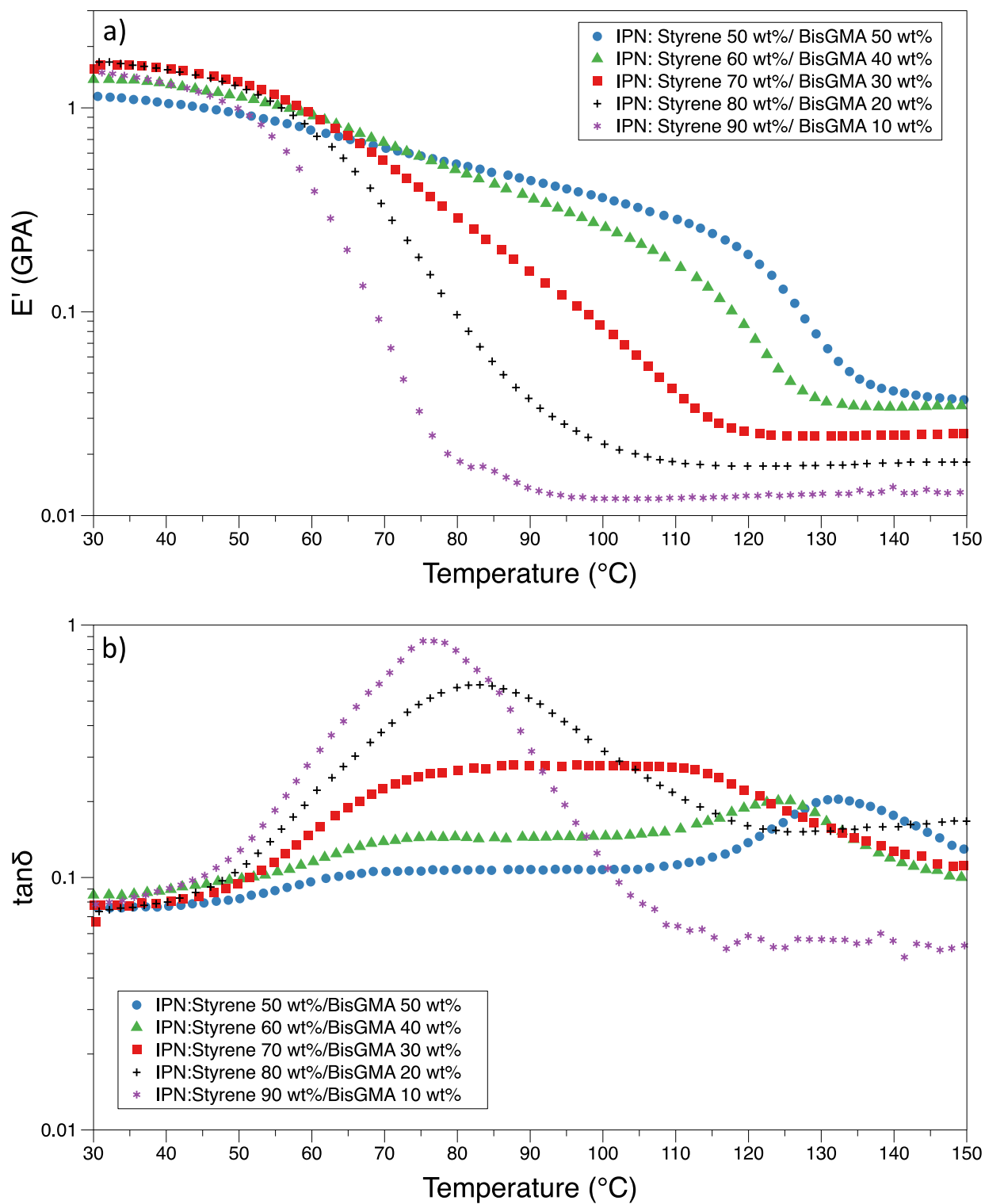


Figure 12. Flexural test results a) storage modulus vs. temperature and b) tan delta vs. temperature for IPNs with 25 wt% PU and 75 wt% acrylic copolymer with varied acrylic copolymer precursors.

Fracture Properties

Fracture toughness of the copolymer with 80 wt% styrene and 20 wt% BisGMA (COP80/20) and IPN with 75 wt% copolymer (80 wt% styrene) and 25 wt% PU (IPN80/20) were characterized, and a representative load vs. displacement plot is shown in Figure 13. Both samples show a linear elastic response up to the peak load, followed by brittle failure. IPN80/20 exhibited a higher load capacity at failure indicating enhanced fracture toughness and higher extension before brittle failure in comparison to the neat acrylic copolymer. Plane-strain fracture toughness, K_{Ic} of COP80/20 and IPN80/20 were 1.61 ± 0.16 and 2.2 ± 0.19 MPa.m^{1/2}, respectively. IPN80/20 shows approximately 40% improvement in fracture toughness in comparison to COP80/20 as the presence of polyurethane in the system improves the fracture properties by providing additional flexibility. Moreover, IPN80/20 shows more than 100 % improvement in fracture toughness in contrast to virgin atactic polystyrene with 1.00 ± 0.20 fracture toughness and PMMA with 1.08 ± 0.18 MPa.m^{1/2} fracture toughness.^{41,42}

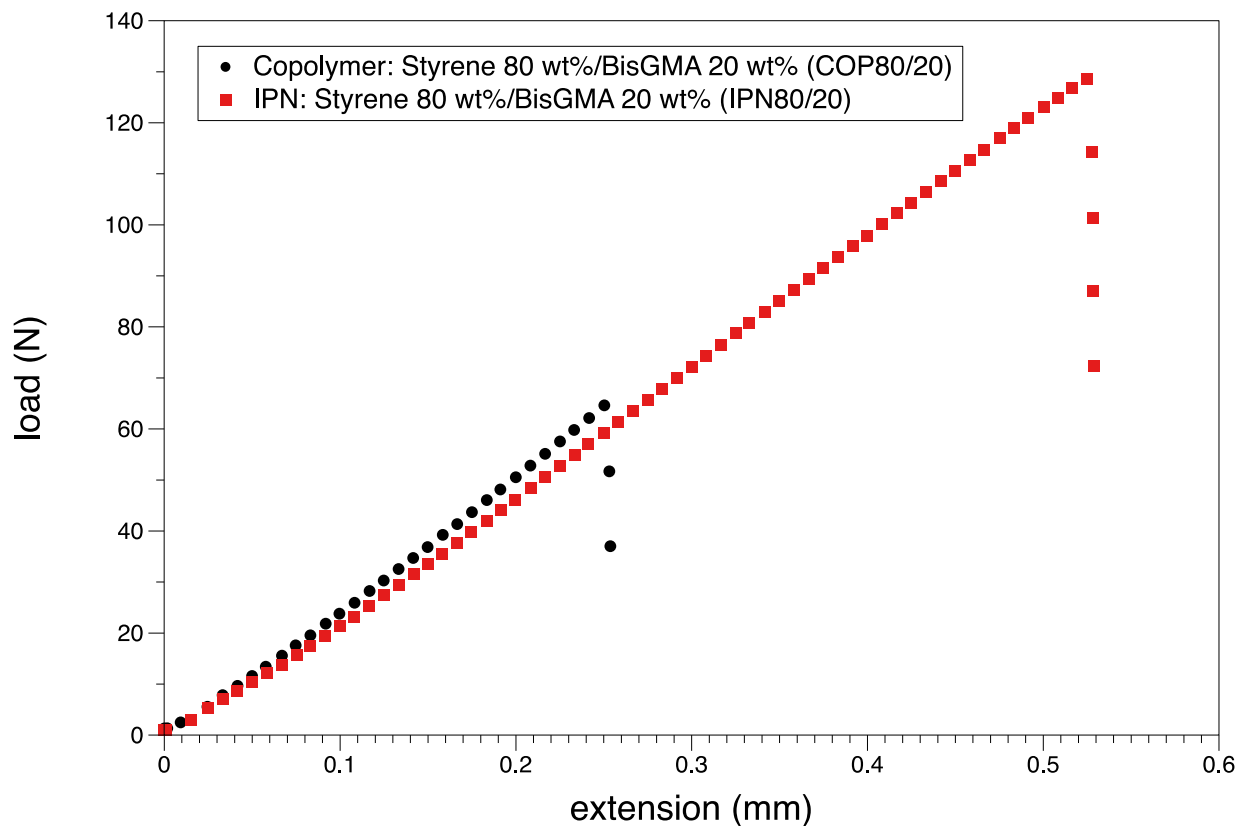


Figure 13. Representative load-displacement plots for acrylic copolymer and IPN with 25 wt% PU and 75 wt% acrylic copolymer.

Scanning electron microscopy (SEM) was used to investigate the fracture mechanism of the synthesized IPNs with varied acrylic network composition. The SEM images of the fractured samples are shown in Figure 14. With increasing styrene content, an observable decrease in the roughness and surface area is observed, corresponding to less energy dissipation during fracture propagation. Although increasing the percentage of styrene increases the compatibility between two phases, it decreases the fracture toughness properties of the samples. Similar behavior has

been observed in the literature where obtaining a rougher surface enhances the fracture toughness properties of the samples.^{20, 43}

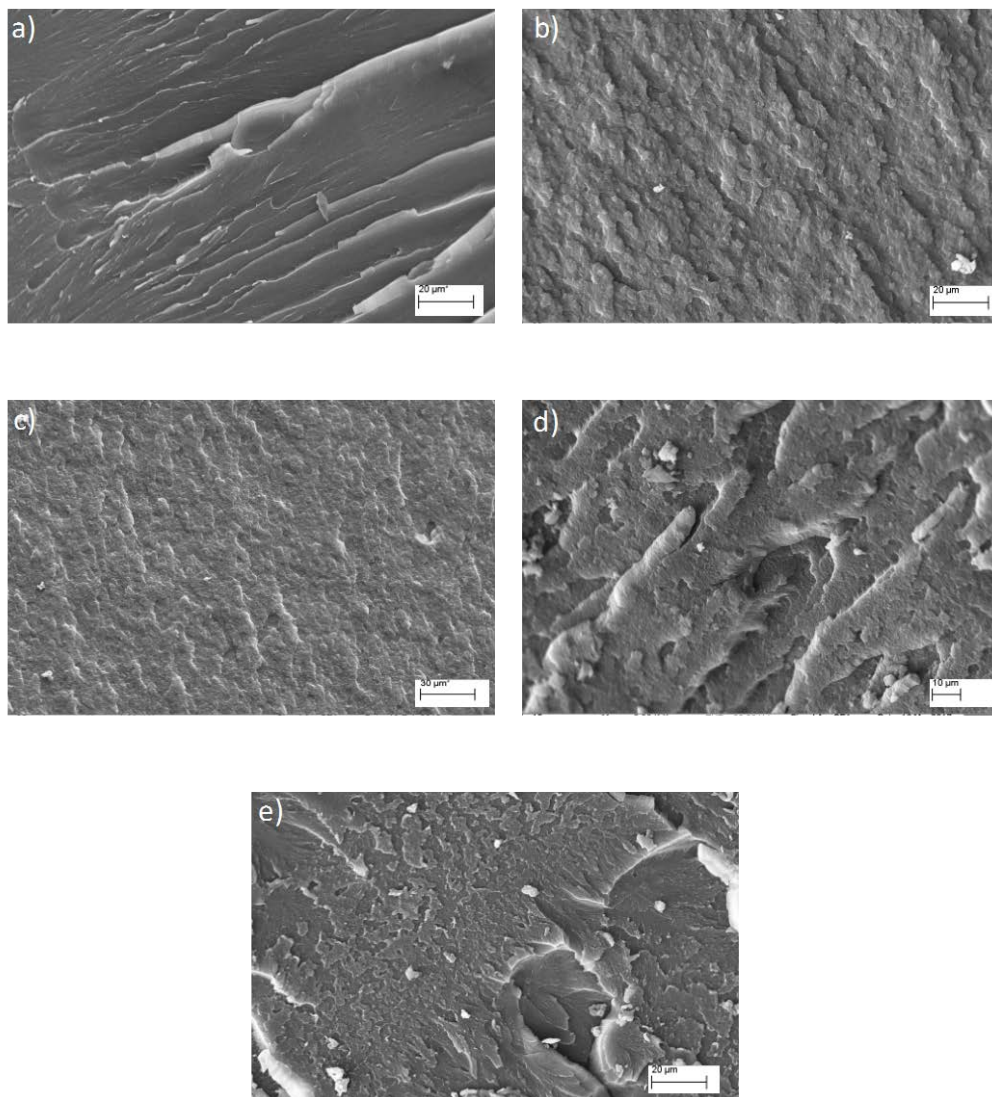


Figure 14. SEM images of **a.** copolymer: Styrene 80 wt%/BisGMA 20wt% and IPN samples with 25 wt% PU and 75 wt% acrylic copolymer with varied acrylic copolymer precursors: b.

IPN: Styrene 50 wt%/BisGMA 50wt% **c.** IPN: Styrene 60 wt%/BisGMA 40wt% **d.** IPN: Styrene 70 wt%/BisGMA 30wt% **e.** IPN: Styrene 80 wt%/BisGMA 20wt%

Conclusions

Acrylic-polyurethane based graft-IPNs were synthesized, and their reaction kinetics, thermo-mechanical, and optical properties investigated. Chemical bonding between the two polymers was utilized to increase the interpenetration between two polymer networks. FTIR spectroscopy revealed complete isocyanate conversion and the formation of polyurethane linkages and chemical bonds between the two polymer networks. ¹H NMR spectroscopy was also utilized to track the kinetics of polyurethane formation, and the results were found to be in good agreement with those from FTIR spectroscopy.

The interplay of IPN composition and related material properties was investigated as a function of IPN styrene content. Incorporation of the acrylic copolymer network provided higher rigidity and better thermomechanical properties to the material. In contrast, higher flexibility was imparted by the polyurethane phase, increasing the impact-resistant and the fracture toughness of the IPNs. DMA, TEM, and UV-VIS spectrophotometry results indicate that increasing the percentage of styrene into the system improves the interpenetration between two polymer networks and therefore enhances the compatibility between two polymer networks. SEM images suggest that increasing the styrene content decreases fracture toughness as observed from the change in surface roughness upon fracture. Significant improvement was observed in fracture toughness of graft-IPN in

comparison to an acrylic copolymer in graft-IPNs. Such graft-IPN with excellent transparency and fracture toughness better than PS and PMMA has considerable potential in high fracture toughness applications.

ACKNOWLEDGMENT

The authors would like to thank NSF-CREST Center for Sustainable Lightweight Materials (C-SLAM) award #1735971 for funding this study.

References

1. Patel, P. J.; Gilde, G. A.; Dehmer, P. G.; McCauley, J. W., Transparent armour. *The AMPTIAC Newsletter* 4 (3) 2000.
2. Kobayashi, A.; Ohtani, N., Dynamic Fracture in Aerospace High Polymers. In *Resins for Aerospace*, AMERICAN CHEMICAL SOCIETY: 1980; Vol. 132, pp 367-377.
3. Martin, A. M. a. G., *Glass: A World History*. The University of Chicago Press: Chicago, USA, 2002.
4. Rawson, H., *Properties and Applications of Glass*. Elsevier Scientific Publishing Co.: 1980.
5. Jajam, K. C.; Bird, S. A.; Auad, M. L.; Tippur, H. V. Tensile, fracture and impact behavior of transparent Interpenetrating Polymer Networks with polyurethane-poly(methyl methacrylate). *Polymer Testing* **2013**, 32 (5), 889-900 DOI: 10.1016/j.polymertesting.2013.04.010.
6. Méndez, R. B. Sequential graft-Interpenetrating polymer networks based on polyurethane and acrylic/ester copolymers. Auburn University, Auburn, AL, 2015.

7. Sundaram, B. M.; Mendez, R. B.; Auad, M. L.; Tippur, H. V. Quasi-static and dynamic mechanical behavior of transparent graft-interpenetrating polymer networks (graft-IPNs). *Polymer Testing* **2018**, 70, 348-362 DOI: <https://doi.org/10.1016/j.polymertesting.2018.06.032>.
8. Robeson, L. M., *Polymer Blends: A Comprehensive Review*. Hanser: 2007.
9. Panapitiya, N. P.; Wijenayake, S. N.; Huang, Y.; Bushdiecker, D.; Nguyen, D.; Ratanawanate, C.; Kalaw, G. J.; Gilpin, C. J.; Musselman, I. H.; Balkus, K. J.; Ferraris, J. P. Stabilization of immiscible polymer blends using structure directing metal organic frameworks (MOFs). *Polymer* **2014**, 55 (8), 2028-2034 DOI: <https://doi.org/10.1016/j.polymer.2014.03.008>.
10. Sperling, L. H.; Mishra, V. The current status of interpenetrating polymer networks. *Polymers for Advanced Technologies* **1996**, 7 (4), 197-208 DOI: Doi 10.1002/(Sici)1099-1581(199604)7:4<197::Aid-Pat514>3.0.Co;2-4.
11. Sperling, L. H.; Klemperer, D.; Utracki, L. A., *Interpenetrating polymer networks*. American Chemical Society: Washington, DC, 1994; p xvi, 638 p.
12. Dave, V. J.; Patel, H. S. Synthesis and characterization of interpenetrating polymer networks from transesterified castor oil based polyurethane and polystyrene. *Journal of Saudi Chemical Society* **2017**, 21 (1), 18-24 DOI: <https://doi.org/10.1016/j.jscs.2013.08.001>.
13. Sheu, H. R.; El-Aasser, M. S.; Vanderhoff, J. W. Phase separation in polystyrene latex interpenetrating polymer networks. *Journal of Polymer Science Part A: Polymer Chemistry* **1990**, 28 (3), 629-651 DOI: 10.1002/pola.1990.080280314.
14. Pissis, P.; Georgoussis, G.; Bershtein, V. A.; Neagu, E.; Fainleib, A. M. Dielectric studies in homogeneous and heterogeneous polyurethane/polycyanurate interpenetrating polymer networks. *Journal of Non-Crystalline Solids* **2002**, 305 (1), 150-158 DOI: [https://doi.org/10.1016/S0022-3093\(02\)01091-8](https://doi.org/10.1016/S0022-3093(02)01091-8).
15. Sperling, L. H., *Interpenetrating Polymer Networks and Related Materials*. Plenum Press, New York, 1981; Vol. 12 (1).
16. Sperling, L. H. Interpenetrating polymer networks and related materials. **1977**, 12 (1), 141-180 DOI: doi:10.1002/pol.1977.230120103.
17. Sperling, L. H., Interpenetrating Polymer Networks: An Overview. In *Interpenetrating Polymer Networks*, American Chemical Society: 1994; Vol. 239, pp 3-38.
18. Mita, I.; Akiyama, S., *Molecular Design of Network Polymers*, in *Macromolecular Design of Polymeric Materials*. Marcel Dekker, Inc.: 1997; p 400.
19. Millar, J. R. 263. Interpenetrating polymer networks. Styrene-divinylbenzene copolymers with two and three interpenetrating networks, and their sulphonates. *Journal of the Chemical Society (Resumed)* **1960**, (0), 1311-1317 DOI: 10.1039/JR9600001311.
20. Chen, C. H.; Chen, W. J.; Chen, M. H.; Li, Y. M. Simultaneous full-interpenetrating polymer networks of blocked polyurethane and vinyl ester Part I. Synthesis, swelling ratio, thermal properties and morphology. *Polymer* **2000**, 41 (22), 7961-7967 DOI: Doi 10.1016/S0032-3861(00)00173-7.

21. Fan, L. H.; Hu, C. P.; Ying, S. K. Thermal analysis during the formation of polyurethane and vinyl ester resin interpenetrating polymer networks. *Polymer* **1996**, 37 (6), 975-981 DOI: Doi 10.1016/0032-3861(96)87280-6.
22. Sundararajan, S.; Samui, A. B.; Kulkarni, P. S. Interpenetrating phase change polymer networks based on crosslinked polyethylene glycol and poly(hydroxyethyl methacrylate). *Solar Energy Materials and Solar Cells* **2016**, 149, 266-274 DOI: <https://doi.org/10.1016/j.solmat.2015.12.040>.
23. Sibaja, B.; Matheus, C. P.; Mendez, R. B.; Vega-Baudrit, J. R.; Auad, M. L. Synthesis and Characterization of Interpenetrating Polymer Networks (IPNs) from Acrylated Soybean Oil and α -Resorcylic Acid: Part 1. Kinetics of Network Formation. *Journal of Renewable Materials* **2017**, 5 (3-4), 231-240 DOI: 10.7569/JRM.2017.634113.
24. Sibaja, B.; Matheus, C. P.; Mendez, R. B.; Farag, R.; Baudrit, J. R. V.; Auad, M. L. Synthesis and Characterization of Interpenetrating Polymer Networks (IPNs) from Acrylated Soybean Oil α -Resorcylic Acid: Part 2. Thermo-Mechanical Properties and Linear Fracture Mechanics. *Journal of Renewable Materials* **2017**, 5 (3-4), 241-250 DOI: 10.7569/JRM.2017.634114.
25. Bird, S. A.; Clary, D.; Jajam, K. C.; Tippur, H. V.; Auad, M. L. Synthesis and characterization of high performance, transparent interpenetrating polymer networks with polyurethane and poly(methyl methacrylate). *Polymer Engineering & Science* **2013**, 53 (4), 716-723 DOI: 10.1002/pen.23305.
26. Jajam, K. C.; Tippur, H. V.; Bird, S. A.; Auad, M. L. In *Dynamic Fracture and Impact Energy Absorption Characteristics of PMMA-PU Transparent Interpenetrating Polymer Networks (IPNs)*, Dynamic Behavior of Materials, Volume 1, Cham, 2014//, 2014; Song, B., Casem, D., Kimberley, J., Eds. Springer International Publishing: Cham, 2014; pp 277-284.
27. Jajam, K. C.; Bird, S. A.; Auad, M. L.; Tippur, H. V. In *Development and Characterization of a PU-PMMA Transparent Interpenetrating Polymer Networks (t-IPNs)*, Dynamic Behavior of Materials, Volume 1, New York, NY, 2011//, 2011; Proulx, T., Ed. Springer New York: New York, NY, 2011; pp 117-121.
28. Ballesteros, R.; Sundaram, B. M.; Tippur, H. V.; Auad, M. L. Sequential graft-interpenetrating polymer networks based on polyurethane and acrylic/ester copolymers. *Express Polymer Letters* **2016**, 10 (3), 204-215 DOI: 10.3144/expresspolymlett.2016.19.
29. Hillerström, A.; Andersson, M.; Pedersen, J. S.; Altskär, A.; Langton, M.; van Stam, J.; Kronberg, B. Transparency and wettability of PVP/PDMS-IPN synthesized in different organic solvents. *Journal of Applied Polymer Science* **2009**, 114 (3), 1828-1839 DOI: 10.1002/app.30673.
30. Qin, C.-L.; Cai, W.-M.; Cai, J.; Tang, D.-Y.; Zhang, J.-S.; Qin, M. Damping properties and morphology of polyurethane/vinyl ester resin interpenetrating polymer network. *Materials Chemistry and Physics* **2004**, 85 (2-3), 402-409 DOI: 10.1016/j.matchemphys.2004.01.019.
31. Alizadeh, N.; Bird, S. A.; Mendez, R. B.; Jajam, K. C.; Alexander, A. C.; Tippur, H. V.; Auad, M. L., Chapter 11 - Synthesis and Characterization of High Performance Interpenetrating

Polymer Networks With Polyurethane and Poly(methyl methacrylate). In *Unsaturated Polyester Resins*, Elsevier: 2019; pp 243-255.

32. Bird, S. A. Interpenetrating Polymer Networks with Polyurethane and Methacrylate-based Polymers. Auburn University, Auburn, AL, 2013.
33. Huang, J.; Zhang, L. Effects of NCO/OH molar ratio on structure and properties of graft-interpenetrating polymer networks from polyurethane and nitrolignin. *Polymer* **2002**, 43 (8), 2287-2294 DOI: [https://doi.org/10.1016/S0032-3861\(02\)00028-9](https://doi.org/10.1016/S0032-3861(02)00028-9).
34. Kato, K. Osmium tetroxide fixation of rubber latices. *Journal of Polymer Science Part B: Polymer Letters* **1966**, 4 (1), 35-38 DOI: 10.1002/pol.1966.110040107.
35. Standard Test Methods for Plane-Strain Fracture Toughness and Strain Energy Release Rate of Plastic Materials.
36. Pavia, D. L.; Lampman, G. M.; Kriz, G. S., *Introduction to spectroscopy, Third edition*. Thomson Learning: Washington, 2001.
37. Cateto, C. A.; Barreiro, M. F.; Rodrigues, A. E. Monitoring of lignin-based polyurethane synthesis by FTIR-ATR. *Industrial Crops and Products* **2008**, 27 (2), 168-174 DOI: 10.1016/j.indcrop.2007.07.018.
38. Anslyn, E. V.; Dougherty, D. A.; Sausalito, C. U. S., *Modern physical organic chemistry*. University Science Books www.uscibooks.com: CA, 2006.
39. Chakrapani, S. B.; Minkler, M. J.; Beckingham, B. S. Low-field ¹H-NMR spectroscopy for compositional analysis of multi-component polymer systems. *Analyst* **2019**, 144 (5), 1679-1686 DOI: 10.1039/C8AN01810C.
40. Auad, M. L.; Aranguren, M.; Borrajo, J. Epoxy-based divinyl ester resin/styrene copolymers: Composition dependence of the mechanical and thermal properties. *Journal of Applied Polymer Science* **1997**, 66 (6), 1059-1066 DOI: 10.1002/(SICI)1097-4628(19971107)66:6<1059::AID-APP6>3.0.CO;2-H.
41. Serrano, A.; Welsch, G.; Gibala, R. Fracture toughness and fatigue of polystyrene, polyphenylene oxide and their blends. *Polymer Engineering & Science* **1982**, 22 (15), 946-949.
42. Choi, S. R.; Salem, J. A. Fracture toughness of PMMA as measured with indentation cracks. *Journal of Materials Research* **1993**, 8 (12), 3210-3217 DOI: 10.1557/JMR.1993.3210.
43. Hsieh, K. H.; Han, J. L.; Yu, C. T.; Fu, S. C. Graft interpenetrating polymer networks of urethane-modified bismaleimide and epoxy (I): mechanical behavior and morphology. *Polymer* **2001**, 42 (6), 2491-2500 DOI: Doi 10.1016/S0032-3861(00)00641-8.